CrossMark

ARTICLE

Dispersion of a Passive Scalar Fluctuating Plume in a Turbulent Boundary Layer. Part II: Analytical Modelling

Massimo Marro[1] · **Chiara Nironi**[1] · **Pietro Salizzoni**[1] ·
Lionel Soulhac[1]

Abstract We investigate the reliability of a meandering plume model in reproducing the passive scalar concentration statistics due to a continuous release in a turbulent boundary layer. More specifically, we aim to verify the physical consistency of the parametrizations adopted in the model through a systematic comparison with experimental data. In order to perform this verification, we take advantage of the velocity and concentration measurements presented in part I of the present study (Nironi et al., Boundary-Layer Meteorol, 2015) particularly concerning estimates of the Eulerian integral length scales and the higher order moments of the concentration probability density function. The study is completed by a sensitivity analysis in order to estimate the effects of the variations of the key parameter to the model results. In the light of these results, we discuss the benefits and shortcomings of this modelling approach and its suitability for operational purposes.

Keywords Atmospheric turbulence · Concentration · Fluctuating plume · Meandering · Pollutant dispersion · Probability density function · Relative dispersion

1 Introduction

Fluctuating plume dispersion models are conceived to estimate the concentration statistics of a pollutant dispersing within a turbulent flow. Compared to other modelling approaches, such as micro-mixing Lagrangian models (Sawford 2004; Cassiani et al. 2005; Leuzzi et al. 2012; Amicarelli et al. 2012; Cassiani 2013) and large-eddy simulations (Xie et al. 2004; Vinkovic et al. 2006), their relatively simple formulation makes them suitable for operational purposes.

✉ Pietro Salizzoni
pietro.salizzoni@ec-lyon.fr

1 Laboratoire de Mécanique des Fluides et d'Acoustique, University of Lyon, CNRS UMR 5509,
Ecole Centrale de Lyon, INSA Lyon, Université Claude Bernard, 36, avenue Guy de Collongue,
69134 Ecully, France

The basic principle of this modelling approach (Gifford 1959) is to split the total plume dispersion into two components: meandering and relative dispersion. The first mechanism describes the fluctuation of the plume centroid, whereas the relative dispersion drives the spreading of a plume element around its centre of mass. The two mechanisms can be treated as independent, as long as it is assumed that they are related to spatial scales separated by several orders of magnitude. As pointed out by Yee et al. (1994), and as discussed later, this hypothesis is strictly valid only close to the source or in the far field. In between there does not exist a clear spectral gap between the scales of motion contributing to the plume meandering and those associated with the relative dispersion. Despite this theoretical weakness, this modelling approach was shown to be quite robust in simulating the dispersion of a passive scalar in a variety of turbulent flows (Fackrell and Robins 1982; Sawford and Stapountzis 1986; Yee et al. 1994; Franzese 2003).

Adopting this assumption, the concentration probability density function (PDF), p, can be written as the convolution of the PDF of the location of the cloud instantaneous centroid, p_m, characterizing the large-scale random crosswind displacements of the centre of mass, and the PDF of the concentration in the meandering reference scheme (y_m, z_m), p_{cr},

$$p(c; x, y, z) = \int_0^\infty \int_{-\infty}^\infty p_{cr}(c; x, y, z, y_m, z_m)\, p_m(x, y_m, z_m) \mathrm{d}y_m \mathrm{d}z_m, \tag{1}$$

where c is the instantaneous concentration. Once p is known, the moments of the concentration can be computed as,

$$\overline{c^n}(x, y, z) = \int_0^\infty c^n p(c; x, y, z) \mathrm{d}c. \tag{2}$$

The practice of partitioning the concentration fluctuations depending on the their characteristic length scales was originally introduced by Gifford (1959). He proposed a model for dispersion in isotropic and homogeneous turbulence, neglecting the role of internal concentration fluctuations, so that p_{cr} was parametrized by the Dirac delta function δ_D,

$$p_{cr}(c; x, y, z, y_m, z_m) = \delta_D \{c - \overline{c}_r(x, y, z, y_m, z_m)\}, \tag{3}$$

where $\overline{c}_r$ is the mean concentration relative to the instantaneous plume centroid. The assumption of negligible internal fluctuations is reliable for short times, so far as meandering is the mechanism governing the dispersion process. It becomes unrealistic in the far field, where the role of relative dispersion overcomes that of meandering.

This relatively simple model was shown to reliably predict the main features characterizing the near-field dynamics of a fluctuating plume emitted from an elevated source. Fackrell and Robins (1982) simulated the effect of a varying source size on the intensity of the concentration fluctuation in an anisotropic and non-homogeneous velocity field. According to their analysis, this can be attributed to the different role of the meandering motion, whose intensity increases as the source size decreases, since the range of scales of the turbulent motion, that are responsible for displacing the plume centre of mass, widens. The model is also able to distinguish between the different shapes that the concentration PDF assumes according to the type of source (Sawford and Stapountzis 1986), predicting a unimodal PDF for the point source and a bimodal PDF for the line source, in agreement with experimental observations.

The role of the relative in-plume fluctuations was firstly taken into account by Yee et al. (1994) who introduced the intensity of the relative concentration fluctuations i_{cr} as a new parameter, defined as the ratio between the standard deviation of the mean relative concen-

tration, σ_{cr}, and $\overline{c}_r$. The overall statistics of the relative dispersion were then parametrized by means of a Gamma distribution,

$$p_{cr}(c; x, y, z, y_m, z_m) = \frac{\lambda^\lambda}{\overline{c}_r \Gamma(\lambda)} \left(\frac{c}{\overline{c}_r} \right)^{\lambda - 1} \exp\left(-\frac{\lambda c}{\overline{c}_r} \right), \tag{4}$$

where $\Gamma(\lambda)$ is the gamma function and $\lambda = 1/i_{cr}^2$. A one-dimensional formulation of the model was tested against in situ measurements of concentrations (Yee et al. 1994) at different heights above the ground within an atmospheric boundary layer over a uniform flat terrain. A two-dimensional formulation of the model for homogeneous and isotropic turbulence was tested by Yee and Wilson (2000) against water-plume measurements of the first four moments of the concentration PDF of a passive scalar dispersing in grid turbulence. In order to reliably model the anisotropy and the inhomogeneity of the velocity field within a turbulent boundary layer, several authors (Reynolds 2000; Luhar et al. 2000; Franzese 2003; Mortarini et al. 2009) have reconstructed the spatial evolution of the vertical component of the plume centroid PDF, p_{zm}, by means of stochastic Lagrangian models simulating the trajectories of the puff centre of mass. Cassiani and Giostra (2002) have also developed a generalized approach that allows p_{zm} to be computed by means of a mean concentration field, without the need for a Lagrangian particle model. All the above-mentioned models include a simple formulation of i_{cr} that is assumed to depend on the longitudinal coordinate only. More complex parametrizations of i_{cr} have been proposed only recently. Gailis et al. (2007) introduced a three-dimensional model of i_{cr} to predict the concentration PDF within a dispersion plume in a group of obstacles. This same parametrization was used by Ferrero et al. (2013) to compute the concentration statistics of two reactive chemical species within a convective boundary layer.

In this paper, we present a formulation of the fluctuating plume model (Sect. 2) and discuss the parametrizations that render the model suitable for simulating the dispersion process within a turbulent neutral boundary layer (Sect. 3). In particular, we aim to analyze the consistency of these parametrizations in the light of the experimental characterization of the velocity field performed by Nironi et al. (2015), especially concerning the estimates of the Eulerian integral length scales (Sect. 3.1). Subsequently, the focus is on i_{cr} (Sect. 3.2) that is modelled adopting two different parametrizations. Assuming $i_{cr} = i_{cr}(x)$ (Sect. 3.2.1), the formulation of the meandering model leads to an analytical solution for $p(c; x, y, z)$, whereas assuming $i_{cr} = i_{cr}(x, y, z)$ (Sect. 3.2.2) leads to a semi-analytical solution. Both formulations are compared to the experimental wind-tunnel results of Nironi et al. (2015), providing a unique dataset concerning the spatial distribution of the first four moments of the concentration PDF (Sect. 4). Finally we perform an error and sensitivity analysis of several key parameters (Sect. 5) to determine the robustness and accuracy of the model and discuss its advantages and shortcomings, as well as its suitability for operational purposes (Sect. 6).

2 Meandering Plume Model

We consider a source of diameter σ_0 located at coordinates $(0, y_s, z_s)$ within a turbulent boundary layer of depth δ. Following Yee and Wilson (2000) and Luhar et al. (2000) we assume the statistical independence of the plume meandering in the lateral and vertical directions, so that p_m can be expressed as the product of two components, p_{ym} and p_{zm},

$$p_m(x, y_m, z_m) = p_{ym}(x, y_m) p_{zm}(x, z_m). \tag{5}$$

We stress here that this assumption is not supported by any theoretical consideration, but is rather justified by the need for simplicity in the formulation of the model.

Since the velocity statistics are assumed to be homogeneous in the horizontal planes, the crosswind distribution of the centroid locations is Gaussian,

$$p_{ym}(x, y_m) = \frac{1}{\sqrt{2\pi}\sigma_{ym}} \exp\left(-\frac{(y_m - y_s)^2}{2\sigma_{ym}^2}\right), \tag{6}$$

where σ_{ym} is the centroid horizontal spread.

Conversely, p_{zm} requires a slightly more complex formulation in order to account for the effects of ground reflection and the non-homogeneity of the velocity statistics in the vertical direction. This is modelled by means of the following reflected Gaussian distribution (Arya 1999),

$$p_{zm}(x, z_m) = \frac{1}{\sqrt{2\pi}\sigma_{zm}} \left\{ \exp\left[-\frac{(z_m - z_s)^2}{2\sigma_{zm}^2}\right] + \exp\left[-\frac{(z_m + z_s)^2}{2\sigma_{zm}^2}\right] \right\}, \tag{7}$$

where σ_{zm} is the vertical spread of the plume centroid. In the presence of one boundary, a reflected Gaussian ensures a constant mass flux $\int_0^\infty p_{zm}\mathrm{d}z_m = 1$ through any vertical section perpendicular to the wind direction, a constraint that is not satisfied by a simple Gaussian model far from the source, which gives

$$\frac{1}{\sqrt{2\pi}\sigma_{zm}} \int_0^\infty \exp\left(-\frac{(z_m - z_s)^2}{2\sigma_{zm}^2}\right)\mathrm{d}z_m = \frac{1}{2}\left(1 + \mathrm{erf}\left(\frac{z_s}{\sqrt{2}\sigma_{zm}}\right)\right) \le 1. \tag{8}$$

Note that different atmospheric stability conditions can alter significantly the shape of p_{zm}. For a detailed discussion on this topic, see Luhar et al. (2000) and Franzese (2003).

Similarly, to account for the anisotropy of the relative dispersion, we parametrize the relative mean concentration $\bar{c}_r$ as

$$\bar{c}_r = \frac{M_q}{\bar{u}_m} p_{yr}(x, y, y_m)\, p_{zr}(x, z, z_m), \tag{9}$$

where M_q is the mass flow rate and $\bar{u}_m = \bar{u}(\bar{z}_m)$ is the mean cloud advection velocity. This parameter, as well as all other velocity statistics—mean velocity, velocity variances and turbulent kinetic energy (TKE) dissipation rate—used in the model, is evaluated at the plume centroid $\bar{z}_m(x)$ and therefore depends solely on the downwind distance from the source. The implications of this assumption on the results are discussed in Sect. 5.2. The functions p_{yr} and p_{zr} are the lateral and vertical distributions of the mean concentration around the plume centroid and are modelled as,

$$p_{yr} = \frac{1}{\sqrt{2\pi}\sigma_{yr}} \exp\left(-\frac{(y - y_m)^2}{2\sigma_{yr}^2}\right), \tag{10}$$

$$p_{zr} = \frac{1}{\sqrt{2\pi}\sigma_{zr}} \left\{ \exp\left(-\frac{(z - z_m)^2}{2\sigma_{zr}^2}\right) + \exp\left(-\frac{(z + z_m)^2}{2\sigma_{zr}^2}\right) \right\}, \tag{11}$$

where σ_{yr} and σ_{zr} are the relative plume spreads around the plume's centre of mass in the horizontal and vertical directions, respectively.

Substituting Eqs. 4, 6, 7 and 9 into Eq. 2 and solving the integral in the variable c, we obtain the n-th concentration moment as function of the position in space (x, y, z),

$$
\begin{aligned}
\overline{c^n}(x, y, z) &= \int_0^\infty p_{zm}\, \mathrm{d}z_m \int_{-\infty}^\infty p_{ym}\, \mathrm{d}y_m \int_0^\infty c^n\, p_{cr}(c; x, y, z, y_m, z_m)\, \mathrm{d}c \\
&= \int_0^\infty p_{zm}\, \mathrm{d}z_m \int_{-\infty}^\infty \frac{1}{\lambda^n} \frac{\Gamma(n+\lambda)}{\Gamma(\lambda)} \overline{c}_r^n\, p_{ym}\, \mathrm{d}y_m \\
&= \left(\frac{M_q}{2\pi \sigma_{yr}\sigma_{zr}\overline{u}_m}\right)^n \frac{1}{2\pi \sigma_{ym}\sigma_{zm}} \\
&\quad \times \int_{-\infty}^\infty \exp\left(-\frac{(y_m - y_s)^2}{2\sigma_{ym}^2}\right) \exp\left(-\frac{n\,(y - y_m)^2}{2\sigma_{yr}^2}\right) \mathrm{d}y_m \\
&\quad \times \int_0^\infty \frac{1}{\lambda^n} \frac{\Gamma(n+\lambda)}{\Gamma(\lambda)} \left\{ \exp\left(-\frac{(z_m - z_s)^2}{2\sigma_{zm}^2}\right) + \exp\left(-\frac{(z_m + z_s)^2}{2\sigma_{zm}^2}\right)\right\} \\
&\quad \times \left\{ \exp\left(-\frac{(z - z_m)^2}{2\sigma_{zr}^2}\right) + \exp\left(-\frac{(z + z_m)^2}{2\sigma_{zr}^2}\right)\right\}^n \mathrm{d}z_m .
\end{aligned}
\tag{12}
$$

In Sect. 3.2 we provide analytical and semi-analytical solutions of Eq. 12, depending on the formulation of $\lambda = 1/i_{cr}^2$.

3 Set of Model Parameters

In order to have a complete formulation of the model, we need to parametrize σ_y, σ_{yr}, σ_{ym}, σ_z, σ_{zr}, σ_{zm}, and i_{cr}. To this end, we take advantage of the information provided by the experimental investigation of the velocity and concentration field presented in Nironi et al. (2015). The analysis is performed for the emissions released from three different sources of varying size σ_0/δ and elevation z_s/δ (see Table 1).

3.1 Parametrization of the Plume Spreads

The global plume spreads are related to the spread of the plume centroid and to the relative spread by the following relations (Gifford 1959),

$$
\sigma_y^2 = \sigma_{ym}^2 + \sigma_{yr}^2,
\tag{13}
$$
$$
\sigma_z^2 = \sigma_{zm}^2 + \sigma_{zr}^2.
\tag{14}
$$

There are therefore two independent plume spread parameters that have to be set. Following Luhar et al. (2000) and Franzese (2003) we model the global spreads σ_y and σ_z, the relative spreads σ_{yr} and σ_{zr}, and then obtain σ_{ym} and σ_{zm} by means of Eqs. 13 and 14.

Table 1 Diameter σ_0 and height z_s of the three sources

	σ_0/δ	z_s/δ
Elevated Source ES 3	0.00375	0.19
Elevated Source ES 6	0.0075	0.19
Low-Level Source LLS	0.00375	0.06

The global spreads are parametrized according to Taylor's statistical theory as Nironi et al. (2015),

$$\sigma_y^2 = \frac{\sigma_0^2}{6} + 2\sigma_v^2 T_{Lv} \left\{ t - T_{Lv} \left[1 - \exp\left(-\frac{t}{T_{Lv}}\right) \right] \right\}, \tag{15}$$

$$\sigma_z^2 = \frac{\sigma_0^2}{6} + 2\sigma_w^2 T_{Lw} \left\{ t - T_{Lw} \left[1 - \exp\left(-\frac{t}{T_{Lw}}\right) \right] \right\}, \tag{16}$$

where σ_v and σ_w are the standard deviations of the transverse and vertical velocity component, T_{Lv} and T_{Lw} are Lagrangian time scales, and $t = x/\overline{u}_m$ is the flight time. As is customary (Tennekes 1982), the Lagrangian time scales are parametrized as $T_{Lv} = \frac{2\sigma_v^2}{C_0 \varepsilon}$ and $T_{Lw} = \frac{2\sigma_w^2}{C_0 \varepsilon}$, where C_0 is the Kolmogorov constant assumed here equal to 4.5 (Nironi et al. 2015), and ε is the mean dissipation rate of the TKE.

The parametrization of the relative dispersion coefficients, σ_{yr} and σ_{zr}, has to satisfy two asymptotic conditions (for brevity we report only those of σ_{yr}, since the same conditions are imposed on σ_{zr}, see Franzese 2003; Franzese and Cassiani 2007),

$$t \to 0 \qquad \sigma_{yr}^2 = (C_r/6)\varepsilon (t_s + t)^3, \tag{17}$$

$$t \to \infty \qquad \sigma_{yr}^2 \to \sigma_y^2 = 2\sigma_v^2 T_{Lv} t, \tag{18}$$

where C_r is the Richardson–Obukhov constant and $t_s = \left[\sigma_0^2/(C_r \varepsilon)\right]^{1/3}$ represents the flight time needed by a plume emitted from a virtual point source to expand to the size σ_0.

Equation 17 follows from the Richardson–Obukhov law for a finite source size (Ott and Mann 2000; Franzese and Cassiani 2007) and models the cloud spreading as a function of the flight time t (Richardson 1926) and ε (Obukhov 1941). Equation 18 is the Taylor's limit for large dispersion time, which applies to σ_{yr} (and σ_{zr}) when the meandering process becomes negligible and the relative dispersion approaches the global dispersion. The objective is to define a suitable transition between the two asymptotic behaviours. To that purpose we adopt an approach similar to that proposed by Luhar et al. (2000) and Franzese (2003). In contrast to them, we introduce the time scales T_{my} and T_{mz}. These are needed in order to ensure that the transition from the inertial scaling to the diffusive asymptotic scaling is consistent with the main characteristics of the large-scale dynamics of the velocity field, presented in Nironi et al. (2015). The evolutions of σ_{yr}^2 and σ_{zr}^2 are then modelled as

$$\sigma_{yr}^2 = \frac{(C_r/6)\varepsilon (t_s + t)^3}{\left\{ 1 + \left[(C_r/6)\varepsilon t^2 / \left(2\sigma_v^2 T_{Lv}\right)\right]^{2/5} \right\}^{5/2}} \exp\left[-\left(\frac{t}{T_{my}}\right)^2\right]$$

$$+ \sigma_y^2 \left\{ 1 - \exp\left[-\left(\frac{t}{T_{my}}\right)^2\right] \right\}, \tag{19}$$

$$\sigma_{zr}^2 = \frac{(C_r/6)\varepsilon (t_s + t)^3}{\left\{ 1 + \left[(C_r/6)\varepsilon t^2 / \left(2\sigma_w^2 T_{Lw}\right)\right]^{2/5} \right\}^{5/2}} \exp\left[-\left(\frac{t}{T_{mz}}\right)^2\right]$$

$$+ \sigma_z^2 \left\{ 1 - \exp\left[-\left(\frac{t}{T_{mz}}\right)^2\right] \right\}, \tag{20}$$

so that the spatial evolutions of σ_{yr} and σ_{zr} are therefore a function of the parameters T_{my}, T_{mz} and C_r, whose setting is discussed in the following paragraphs.
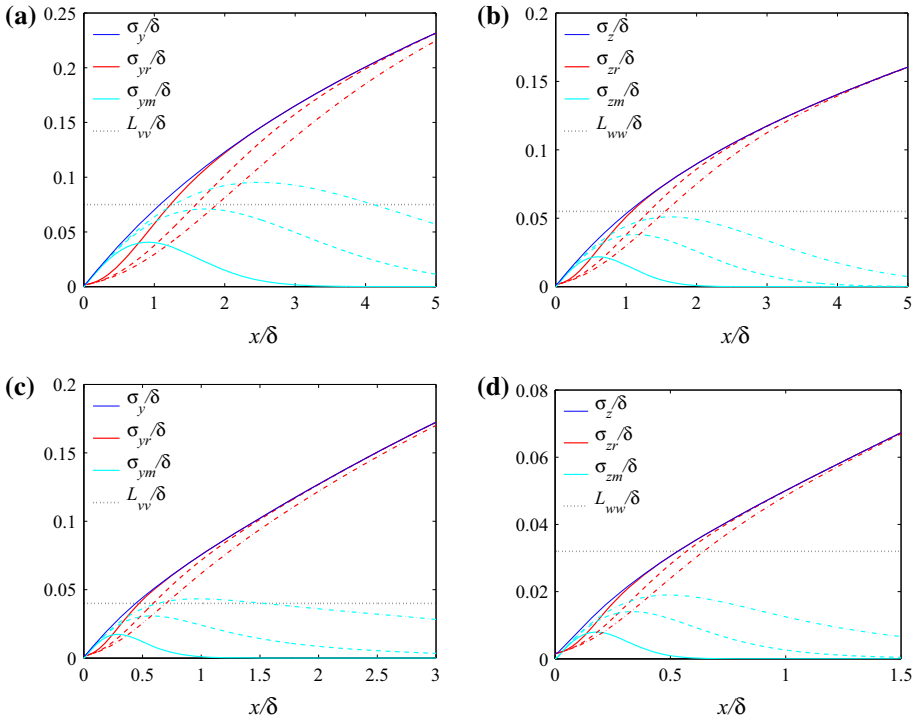
Fig. 1 Modelled transverse and vertical dispersion coefficients varying α_T ($C_0 = 4.5$ and $C_r = 0.8$): **a, b** ES 3 source; **c, d** LLS source. *Solid line $\alpha_T = 1$, dash line $\alpha_T = 2$, dash-dot line $\alpha_T = 3$*. The *black-dotted lines* represent reference values of the Eulerian integral length scales L_{vv} and L_{ww} at source height, as estimated by Nironi et al. (2015)

3.1.1 The Time Scales T_{my} and T_{mz}

The time scales T_{my} and T_{mz} can be thought of as thresholds beyond which relative dispersion becomes the prevalent mechanism. This occurs when the size of the relative plume exceeds that of the largest scale eddies ($\mathcal{L}$), so that the contribution of the TKE to the fluctuations of the cloud centroid becomes negligible. It is questionable if the quantity $\mathcal{L}$ refers to Lagrangian statistics, as proposed by Franzese and Cassiani (2007), or to Eulerian statistics. The latter are adopted here, since we dispose of the direct measurements of the Eulerian integral length scales L_{vv} and L_{ww} (Nironi et al. 2015).

Both T_{my} and T_{mz} are assumed to be proportional to the Lagrangian time scales, $T_{my} = \alpha_{Ty} T_{Lv}$ and $T_{mz} = \alpha_{Tz} T_{Lw}$. In order to define the value of the proportionality coefficients α_{Ty} and α_{Tz}, we analyze the evolution of σ_{yr} and σ_{zr}, as given by Eqs. 19 and 20, and we compare it with the experimental estimates of L_{vv} and L_{ww} evaluated at source height z_s. In doing that, we fix the value of the Richardson–Obukhov constant $C_r = 0.8$ (the sensitivity to C_r is discussed in Sect. 3.1.2). The evolution of σ_{yr} and σ_{zr}, as well as that of σ_{ym} and σ_{zm}, is plotted in Fig. 1 for varying values of $\alpha_{Ty} = \alpha_{Tz} = 1, 2, 3$. As expected, the plot shows that the behaviour of the dispersion coefficients depends on the source elevation. In particular the spreads due to the centre of mass, σ_{ym} and σ_{zm}, for the elevated source ES (Fig. 1a, b) are larger than those of the low-level source LLS (Fig. 1c, d). This can be explained

by two features. Firstly, in the lower part of the boundary layer the size of the most energetic eddies is smaller and, as a consequence, the effects on the dispersion due to the displacement of the plume centroid are significantly reduced. Secondly, the effects of the ground (Luhar et al. 2000; Franzese 2003) result in a more rapid damping of the plume meandering in the vertical direction (Fig. 1b, d) with respect to the transverse coordinate (Fig. 1a, c).

The aim here is to define α_{Ty} and α_{Tz} so that σ_{ym} and σ_{zm} do not exceed L_{vv} and L_{ww}, respectively, (Fig. 1) as σ_{yr} and σ_{zr} attain their asymptotic values. The choice of the most appropriate α_{Ty} and α_{Tz} is somehow arbitrary. In order to constrain the degree of freedom of the model in the parameter space, we impose $\alpha_{Ty} = \alpha_{Tz} = \alpha_T$, a condition that may not be appropriate for any source configurations (as a crosswind line source). Adopting these criteria yields $\alpha_T = 2$. It is worth noting that, in the present case study, the original formulation proposed by Luhar et al. (2000) and Franzese (2003), i.e. without the corrective terms involving T_{my} and T_{mz} in Eqs. 19 and 20, leads to a slower increase of σ_{yr} and σ_{zr} with the distance from the source, implying an unphysical growth of σ_{ym} and σ_{zm} to values exceeding the Eulerian scales. Finally, we point out that the characteristic length scales of the meandering and relative dispersion processes are well-separated only very close to the source and in the far field (where $\sigma_{my}, \sigma_{mz} \to 0$). However, as expected (Fig. 1), this hypothesis is not verified in an intermediate region that actually covers most of the investigated domain, both for the ES and LLS cases.

3.1.2 Richardson–Obukhov Constant C_r

Values of C_r are affected by a significant uncertainty. In homogeneous and isotropic turbulence, estimates obtained with direct numerical simulations are approximately in the range $0.4 < C_r < 0.8$ (Ishihara and Kaneda 2002; Boffetta and Sokolov 2002; Biferale et al. 2005), and in non-homogeneous and anisotropic turbulence the range is further widened. Franzese (2003) adopted $C_r = 1.4$ in a convective boundary layer whereas Mortarini et al. (2009) assumed $C_r = 0.06$ in a plant canopy.

In order to emphasize the influence on the model due to the Richardson–Obukhov constant variations, in Fig. 2 we plot $\frac{\sigma_{ym}}{\sigma_y}$, $\frac{\sigma_{zm}}{\sigma_z}$, $\frac{\sigma_{yr}}{\sigma_y}$, and $\frac{\sigma_{zr}}{\sigma_z}$ as a function of the downwind distance from the source, for values of C_r spanning a range consistent with the literature data, i.e.
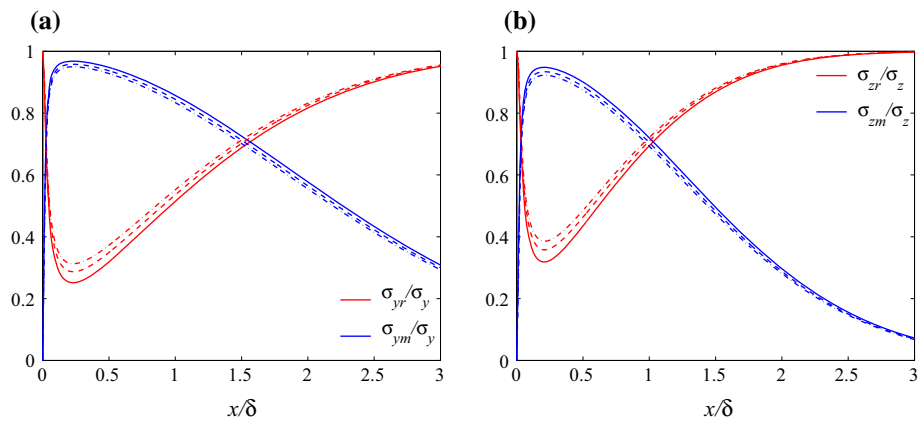

Fig. 2 **a** σ_{yr}/σ_y, σ_{ym}/σ_y, and **b** σ_{zr}/σ_z, σ_{zm}/σ_z vs x/δ for ES 3 varying $C_r = 0.4, 0.8, 1.2$ ($C_0 = 4.5$ and $\alpha_T = 2$); *solid line* $C_r = 0.4$, *dash line* $C_r = 0.8$, *dash-dot line* $C_r = 1.2$

$C_r = 0.4-1.2$. The effects of the variations of C_r are significantly reduced compared to those of α_T, plotted in Fig. 1. Nevertheless, the influence of C_r is non-negligible in an intermediate region (see Fig. 2), from $x/\delta \approx 0.2$ up to $x/\delta \approx 1.5$, within which it can appreciably affect the model results. According to Franzese and Cassiani (2007), the quantity C_r/C_0 should be fixed and equal to $1/11$. Since we adopted $C_0 = 4.5$ this leads to $C_r \approx 0.4$. However, for reasons that will be made clear in the next paragraph (Sect. 3.2), this value was not consistent with the formulation of the model for i_{cr}. We have therefore assumed $C_r = 0.8$ which implies a ratio $C_r/C_0 \approx 0.17$. Note however that this value is quite close to the theoretical value suggested by Franzese and Cassiani (2007) compared to those presented in previous studies (Franzese 2003 imposed $C_r/C_0 \approx 0.5$ and Mortarini et al. 2009 assumed $C_r/C_0 \approx 1/33$).

3.2 Parametrization of the Intensity of Relative Concentration Fluctuations

The determination of the spatial evolution of the intensity of relative concentration fluctuations i_{cr} is a key aspect in the formulation of the meandering models. The dependence of this parameter on the flow dynamics and emission conditions however has been rarely characterized either experimentally or numerically. As far as we know, the only attempt to measure this parameter is that of Gailis et al. (2007), who studied the dispersion of a passive scalar with optical measurement techniques within both a turbulent boundary layer and an obstacle array. Given this lack of information, most of the meandering plume models found in the literature (Luhar et al. 2000; Yee and Wilson 2000; Franzese 2003; Mortarini et al. 2009) adopt quite simple models for i_{cr}, which is generally assumed to be dependent on the x-coordinate only. This assumption however can significantly deteriorate the numerical results in the far field. As shown by Mortarini et al. (2009), to avoid this lack of accuracy of the model it is then necessary to impose an unphysical growth of i_{cr} for increasing distance from the source.

In what follows, we consider two different formulations of the model. In the first case we consider $i_{cr} = i_{cr}(x)$, in the second case $i_{cr} = i_{cr}(x, y, z)$. Both formulations are set in order to ensure the physical consistency of the model with respect to the evolution of the intensity of the concentration fluctuations, $i_c = \sigma_c/\overline{c}$, determined experimentally in the wind-tunnel experiments presented in Nironi et al. (2015).

3.2.1 1-D Model of i_{cr}

In the case of $i_{cr} = i_{cr}(x)$, Eq. 12 can be solved analytically, leading to

$$\overline{c^n}(x, y, z) = \left(\frac{M_q}{2\pi \sigma_{yr}\sigma_{zr}\overline{u}_m}\right)^n \frac{\sigma_{yr}}{\left(n\sigma_{ym}^2 + \sigma_{yr}^2\right)^{0.5}} \frac{\sigma_{zr}}{\left(n\sigma_{zm}^2 + \sigma_{zr}^2\right)^{0.5}} \frac{1}{\lambda^n} \frac{\Gamma(n+\lambda)}{\Gamma(\lambda)}$$

$$\times \exp\left[-\frac{n(y - y_s)^2}{2\left(n\sigma_{ym}^2 + \sigma_{yr}^2\right)}\right] \sum_{k=0}^{n}\left\{\binom{n}{k}\exp\left[-\frac{(n-k)(z - z_s)^2}{2(n\sigma_{zm}^2 + \sigma_{zr}^2)}\right]\right.$$

$$\left. \times \exp\left[-\frac{k(z + z_s)^2}{2(n\sigma_{zm}^2 + \sigma_{zr}^2)}\right]\exp\left[-\frac{(2z)^2 k(n-k)}{2(n\sigma_{zm}^2 + \sigma_{zr}^2)}\frac{\sigma_{zm}^2}{\sigma_{zr}^2}\right]\right\}, \quad (21)$$

where $\binom{n}{k}$ is the binomial coefficient.

With some algebra, Eq. 21 can be rearranged in order to illustrate the relation between i_{cr} and i_c on the plume centreline ($y = y_s, z = z_s$),

$$i_{cr}^2 = \left(i_c^2 + 1\right) F_c - 1, \tag{22a}$$

$$F_c = \frac{\sigma_{yr}\sqrt{2\sigma_{ym}^2 + \sigma_{yr}^2}}{\sigma_y^2} \frac{\sigma_{zr}\sqrt{2\sigma_{zm}^2 + \sigma_{zr}^2}}{\sigma_z^2}$$

$$\times \left\{ 1 + 2\exp\left(-\frac{2(z_s)^2}{(2\sigma_{zm}^2 + \sigma_{zr}^2)}\right) \exp\left(-\frac{2(z_s)^2}{(2\sigma_{zm}^2 + \sigma_{zr}^2)}\frac{\sigma_{zm}^2}{\sigma_{zr}^2}\right) \right.$$

$$\left. + \exp\left(-\frac{4(z_s)^2}{(2\sigma_{zm}^2 + \sigma_{zr}^2)}\right) \right\}^{-1} \left\{ 1 + \exp\left(-\frac{2(z_s)^2}{\sigma_z^2}\right) \right\}^2, \tag{22b}$$

where the evolution of F_c is fully determined by the parametrization (Sect. 3.1) of the plume spreads (total, relative and centroid position). For all release conditions i_c is larger than i_{cr} close to the release point, where the meandering process is significant both for the ES and LLS cases. Moving away from the source, the relative dispersion becomes the prevalent mechanism and $i_{cr} \to i_c$.

As Eq. 22b clearly shows, the model of i_{cr} depends on the distribution of i_c, which therefore requires an independent estimate. To overcome this problem, Yee et al. (1994) and Yee and Wilson (2000) have set i_{cr} by fitting models of the form of Eq. 22b to the experimental estimates of i_c. Following this same approach, we then turn to the experimental values of $i_c(x, y_s, z_s)$ collected by Nironi et al. (2015). By substituting these data in Eq. 22b we determined i_{cr} at six different distances from the source. Since two asymptotic bounds have to be satisfied at source location ($x \to 0$) and in the very far field ($x \to \infty$), the following rational curve was used to fit the i_{cr} estimates,

$$i_{cr} \to 0 \qquad \text{at} \quad \frac{x}{\delta} \to 0, \tag{23a}$$

$$i_{cr} \to i_c = \frac{\sigma_c}{\overline{c}} \neq 0 \qquad \text{at} \quad \frac{x}{\delta} \to \infty, \tag{23b}$$

$$i_{cr} = x_{ad} \frac{p_1 x_{ad}^2 + p_2 x_{ad} + p_3}{x_{ad}^3 + q_1 x_{ad}^2 + q_2 x_{ad} + q_3}, \tag{23c}$$

where $x_{ad} = x/\delta$. The values of the parameters in Eq. 23c for the three cases considered are computed with the method of least-squares and are summarized in Table 2.

As discussed in Sect. 3.1.2, the values of i_{cr} close to the source depend significantly on the choice of C_r (with variations of order 30 %). In particular, for $C_r = 0.4$, we found unphysical negative values of i_{cr}. We have therefore excluded this value, even though it is supported by the theoretical analysis proposed by Franzese and Cassiani (2007), and adopted $C_r = 0.8$ instead.

Figure 3 shows a comparison at increasing distances from the source between the experimental values of i_c, measured on the plume centreline, and the values of i_{cr} computed through

Table 2 Coefficients used in Eq. 23c to calculate i_{cr}

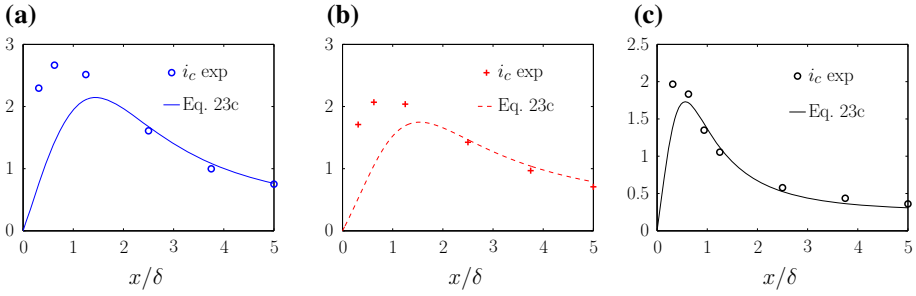|	p_1	p_2	p_3	q_1	q_2	q_3
ES 3	0.35	−1.30	24.54	1.74	−0.58	9.95
ES 6	0.35	0.56	38.64	8.47	−8.70	25.18
LLS	0.35	−0.65	5.97	2.50	−0.55	1.20

Fig. 3 Experimental values of i_c (*symbols*) and i_{cr} computed through Eq. 23c (*lines*) vs x/δ at the plume centreline: **a** ES 3, **b** ES 6, **c** LLS

Eq. 23c. In both ES and LLS cases, i_{cr} exhibits an initial growth and thereafter decreases monotonically to an asymptotic value, which is reached far from the source. As the meandering motion weakens, i_{cr} correctly approaches i_c. In the ES case the meandering influence disappears later ($x/\delta \approx 2$, Fig. 3a, b) in accordance with the model of σ_{ym} and σ_{zm} (Fig. 1). Conversely, in the LLS case the fluctuation of the plume centre of mass is damped very rapidly by the presence of the ground and $i_{cr} \rightarrow i_c$ at $x/\delta \approx 1$ (Fig. 3c). In both cases, the model leads to the same asymptotic value of the relative concentration fluctuations (at $x/\delta \rightarrow \infty$, $i_{cr} \rightarrow 0.35$).

It is worth mentioning that as $i_{cr} \rightarrow i_c$ the intermittency in the core of the plume is suppressed. Note that according to the analysis performed in Sect. 5.3 and Sect. 5.4 in Nironi et al. (2015), this actually takes place at distances ($x/\delta \approx 3.75$ for the ES) that are larger than those predicted by the present model ($x/\delta \approx 2.5$ for the ES, see Fig. 3a, b). In this sense, the model is not fully consistent with the experimental data in this intermediate region between the near and the far field.

As shown in Fig. 3, the model reproduces a dependence of i_{cr} on the source size and elevation. The dependence on z_s is due to the inhomogeneity of the velocity field, whereas the influence of σ_0 is not easily explained. According to this model, the increased intensity i_c observed for the smaller source size is due partially to the increased intensity of the meandering motion and partially to an increased intensity of the relative concentration fluctuations. It is questionable if this trend represents the real physics of the phenomenon or if it has to be attributed to a fictitious effect related to the formulation of the model. The answer to this question, however, can be given only through a direct estimate of i_{cr} by means of experiments or direct numerical simulations.

3.2.2 3-D Model of i_{cr}

By means of experimental measurements, Gailis et al. (2007) showed that the lateral and vertical profiles of i_{cr} exhibit large variations on the y–z plane. Based on these measurements, they proposed to parametrize i_{cr} as a function of the mean relative concentration $\bar{c}_r$,

$$i_{cr}^2(x, y, z) = [1 + i_{cr0}^2(x)] \left[\frac{\bar{c}_r(x, y, z)}{\bar{c}_r(x, y_m, z_m)} \right]^{-\zeta(x)} - 1, \qquad (24)$$

where, for each transverse section corresponding to a given distance x, i_{cr0} is the minimum of i_{cr}, ζ is a shape parameter depending on the longitudinal coordinate and $\bar{c}_r(x, y_m, z_m)$ is the mean relative concentration evaluated at the instantaneous plume centroid. The same
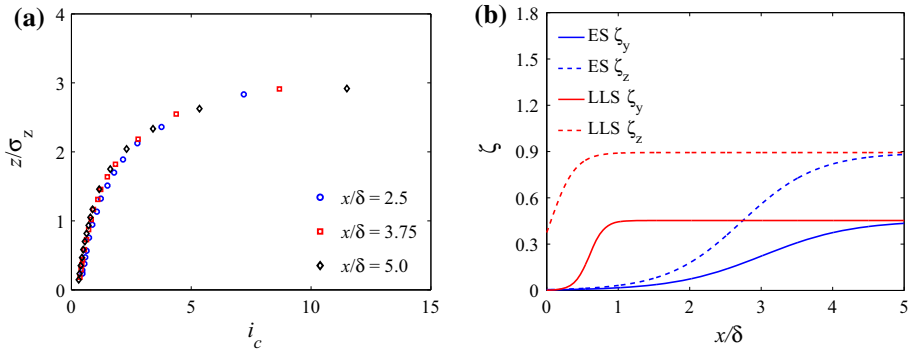
Fig. 4 **a** Self-similarity of the vertical profiles of i_c in the far field, experimental data for the LLS from Nironi et al. (2015); **b** shape parameters ζ_y and ζ_z vs x/δ

parametrization was assumed by Ferrero et al. (2013) in a convective boundary layer. We adopt here a similar formulation, which we slightly modify by introducing two shape parameters, ζ_y and ζ_z, to take into account the effects of anisotropy in the y and z directions,

$$
i_{cr}^2 = (1 + i_{cr0}^2) \left\{ \exp\left(-\frac{(y - y_m)^2}{2\sigma_{yr}^2}\right) \right\}^{-\zeta_y}
$$
$$
\times \left\{ \exp\left(-\frac{(z - z_m)^2}{2\sigma_{zr}^2}\right) + \exp\left(-\frac{(z + z_m)^2}{2\sigma_{zr}^2}\right) \right\}^{-\zeta_z}
$$
$$
\times \left\{ 1 + \exp\left(-\frac{(2z_m)^2}{2\sigma_{zr}^2}\right) \right\}^{\zeta_z} - 1, \tag{25}
$$

where the longitudinal evolution of i_{cr0} remains the same as that defined in the previous paragraph (Sect. 3.2.1).

The evolution of the shape parameters ζ_y and ζ_z with x has been modelled in order to ensure consistency with the main feature characterizing the plume relative dispersion. Close to the source the size of the cloud relative to the plume centroid, σ_{yr} and σ_{zr}, is smaller than the Eulerian integral length scale and mixing with the ambient air is due to eddies whose size ranges from the Kolmogorov scale to that of the cloud itself. We can then expect an efficient mixing within the core of the plume, leading to an almost uniform i_{cr} with respect to y and z directions. Conversely, in the far field σ_{yr} and σ_{zr} approach respectively σ_y and σ_z and exceed significantly the Eulerian integral length scale, so that mixing with ambient air is due to eddies smaller than the plume. The intermittency of the entrainment of ambient air within the plume produces high fluctuations of the relative concentration at the edges of the plume, that are progressively reduced approaching the core. In this case, i_{cr} depends on y- and z-coordinates and the form of its transverse and vertical profiles varies with downwind distance from the source and tends to a self-similar behaviour in the far field. This tendency can be reproduced by modelling the shape parameters with a sigmoid function, viz.

$$
\zeta = \frac{\alpha_1}{\alpha_2 + \exp\left(-\alpha_3 \frac{x}{\delta}\right)}. \tag{26}
$$

Close to the source location $i_{cr}(x) \approx i_{cr0}(x)$ and, therefore, ζ_y and ζ_z should assume values close to zero. The values of α_1 and α_2 have been set in order to fit the self-similar profile of i_c observed experimentally in the LLS case (see Fig. 4a) at large distance from the

Table 3 Sigmoid function coefficients

	LLS		ES	
	ζ_y	ζ_z	ζ_y	ζ_z
α_1	1.43×10^{-3}	0.65	3.58×10^{-3}	5.0×10^{-3}
α_2	3.16×10^{-3}	0.72	7.9×10^{-3}	5.6×10^{-3}
α_3	9.64	5.8	1.6	1.9

Table 4 a_j coefficients evaluated through Eq. 28 for the first four concentration moments

n	a_0	a_1	a_2	a_3
1	1			
2	0	1		
3	0	−1	2	
4	2	2	−7	6

source. The values of α_3 drive the transition between the asymptotic states corresponding to the near and far fields. The spatial extent of this transition is small for the LLS plume, since the profiles of i_c rapidly attain self-similarity, and larger for the ES plume. Therefore, moving away from the source, ζ_y and ζ_z increase and tend to different values, giving an i_{cr} that is shaped differently in the transverse and vertical directions. The values of the coefficients α_1, α_2 and α_3 adopted in our model are reported in Table 3 and the resulting downwind variations of ζ_y and ζ_z are plotted in Fig. 4b.

Substituting Eqs. 25 and 26 in Eq. 12, we obtain an analytical solution in y_m and an integral in z_m, that has to be solved numerically. The moments of the concentration are then given by the following relation,

$$
\overline{c^n}(x, y, z) = \left(\frac{M_q}{2\pi \sigma_{yr} \sigma_{zr} \overline{u}_m}\right)^n \int_0^\infty \sum_{j=0}^{n-1} \left\{ a_j \left[(i_{cr0}^2 + 1) \left(1 + \exp\left(-\frac{4z_m^2}{2\sigma_{zr}^2}\right)\right)^{\zeta_z} \right. \right.
$$

$$
\times \left(\frac{1}{\sqrt{2\pi}\sigma_{zr}\,p_{zr}}\right)^{\zeta_z} \Bigg]^j \frac{\sigma_{yr}}{\sqrt{(n - j\zeta_y)\sigma_{ym}^2 + \sigma_{yr}^2}}
$$

$$
\times \exp\left(-\frac{(n - j\zeta_y)(y - y_s)^2}{2((n - j\zeta_y)\sigma_{ym}^2 + \sigma_{yr}^2)}\right) \Bigg\} \left(\sqrt{2\pi}\sigma_{zr}\,p_{zr}\right)^n p_{zm}\,\mathrm{d}z_m \quad (27)
$$

where a_j are the coefficients of the polynomial

$$
P(x) = \sum_{j=0}^{n-1} a_j x^j = \prod_{k=1}^{n} [(n - k)x - (n - k - 1)] \quad (28)
$$

computable through Vieta's formulae. The values of the coefficients a_j for the first four concentration moments are reported in Table 4.

3.2.3 Asymptotic Behaviour

At large distance from the source ($x/\delta \to \infty$, $t/T_L \to \infty$) the relative dispersion becomes the only mechanism characterizing the dispersion process, so that,
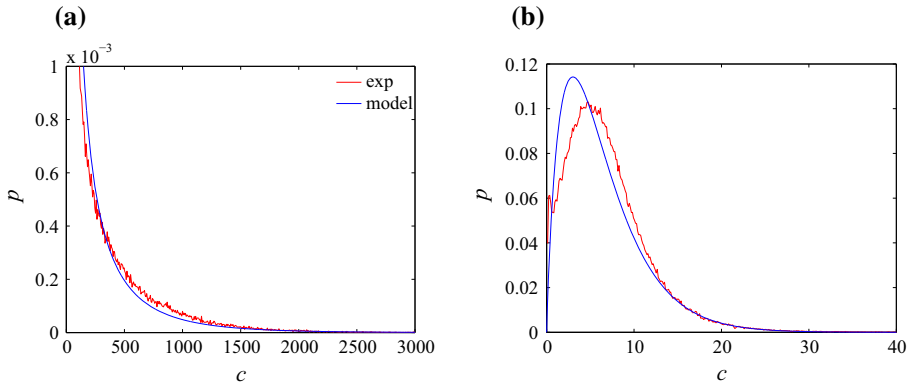
(a)

(b)

Fig. 5 Experimental and modelled PDF on the mean plume centreline varying with the distance from the source location for ES 6 at $y/\delta = 0$, $z/\delta = z_s/\delta$: **a** $x/\delta = 0.625$, **b** $x/\delta = 5.0$

$$i_{cr} \rightarrow i_c, \tag{29a}$$

$$\sigma_{ym} \rightarrow 0, \quad \sigma_{yr} \rightarrow \sigma_y, \tag{29b}$$

$$\sigma_{zm} \rightarrow 0, \quad \sigma_{zr} \rightarrow \sigma_z. \tag{29c}$$

In these conditions, the centroid PDF p_m tends to a Dirac delta distribution and the PDF of the global dispersion (p) is equal to the relative concentration PDF, that assumes the following formulation,

$$p_m \rightarrow \delta_D, \tag{30}$$

$$p_{cr} \rightarrow p = \frac{\lambda^\lambda}{\bar{c}\Gamma(\lambda)} \left(\frac{c}{\bar{c}}\right)^{\lambda-1} \exp\left(-\frac{\lambda c}{\bar{c}}\right) \tag{31}$$

with $\lambda = 1/i_{cr}^2 \rightarrow 1/i_c^2$.

This formulation of the model is in agreement with one of the main findings of the experimental investigation presented in Nironi et al. (2015), i.e. that the PDF of the concentration can be modelled with high accuracy by a Gamma distribution.

4 Comparison with Experimental Results

We finally test the agreement of the fluctuating plume model with the wind-tunnel measurements of the concentration statistics, carried out by Nironi et al. (2015). A first qualitative analysis concerns the form of the concentration PDF at the plume centreline, presented for both formulations of i_{cr} in Sect. 3.2. As an example, in Fig. 5 we report a comparison between the modelled and experimental PDFs at two distances from the source. Close to the source the meandering mechanism prevails (see Fig. 1) and the form of the PDF is similar to a negative exponential distribution (Fig. 5a). In the far field, the meandering becomes negligible with respect to the relative dispersion. The intermittency within the plume is damped, and the shape of the PDF is similar to a log-normal distribution with a short tail, as shown in Fig. 5b. In both cases the model captures the plume dynamics well and accurately reproduces the shape of the concentration PDF.

To perform a more accurate analysis of the model reliability and to quantify the errors in the predictions, we focus on the profiles of the first four moments around the mean, referred
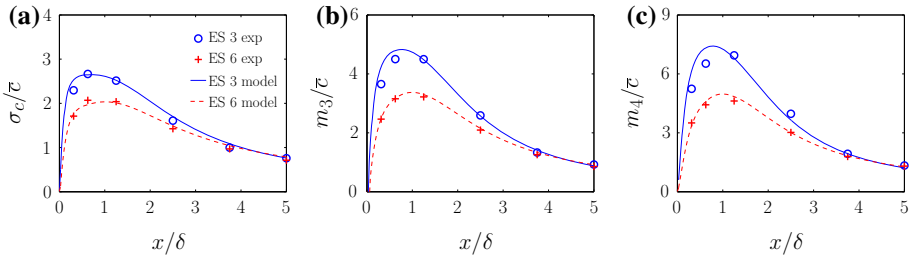
Fig. 6 ES case: concentration statistics vs x/δ at $y/\delta = 0$, $z/\delta = z_s/\delta$: **a** $\sigma_c/\overline{c}$, **b** $m_3/\overline{c}$, **c** $m_4/\overline{c}$

to as m_i, with $i = 1, 2, 3, 4$. These can be computed from Eq. 2 using the following relations (Monin and Yaglom 1971),

$$m_1 = \overline{c}, \tag{32a}$$

$$m_2 = \sigma_c^2 = \overline{c^2} - \overline{c}^2, \tag{32b}$$

$$m_3 = \overline{c^3} - 3\overline{c^2}\overline{c} + 2\overline{c}^3, \tag{32c}$$

$$m_4 = \overline{c^4} - 4\overline{c^3}\overline{c} + 6\overline{c^2}\overline{c}^2 - 3\overline{c}^4. \tag{32d}$$

In the analysis we apply the following normalization:

$$m_i^* = m_i^{1/i} \frac{u_\infty \delta^2}{M_q}, \tag{33}$$

where u_∞ is the velocity at the top of the boundary layer.

It is worth noting that in what follows (as well as in the analysis presented in Sect. 5), the computed values of the first two moments, the mean and the standard deviation, are actually the results of a best fit of the models given by Eq. 21 and Eq. 27 (with $n = 1$ and $n = 2$) to the experimental data, obtained by tuning the model parameters, as discussed in Sect. 3. A real comparison between model and experiments is therefore performed only for m_3^* and m_4^*, whose estimates can be considered as fully independent from the experimental observations.

4.1 Elevated Source

Firstly, we analyze the longitudinal profiles of the ratio between the values of the concentration statistics (σ_c, $m_3^{1/3}$, and $m_4^{1/4}$) and mean concentration $\overline{c}$ at source height, where the estimates of the two models of i_{cr} do not differ one from the other. As Fig. 6 shows, the model provides accurate estimates in the whole domain investigated here ($0 \leq x/\delta \leq 5$), for the two elevated sources considered. In particular, the model reproduces well the influence of the source size in the near field, that progressively vanishes as the meandering motion becomes less effective at displacing the plume centre of mass. The concentration statistics then tend to the same asymptotic values in the far field, independently of the source conditions.

A further analysis concerns the transverse profiles of the concentration statistics at source height. As an example we show in Fig. 7a, c, e, and g a comparison between experiments and model predictions at $x/\delta = 0.625$, $z/\delta = z_s/\delta$. At this distance from the source, the two formulations of the i_{cr} provide almost identical values since $i_{cr} = i_{cr0}$ in both cases. The varying source diameter does not affect the profiles of mean concentration (Fig. 7a), whereas it significantly influences the profiles of the higher order moments (Fig. 7c, e, g). The model results are in excellent agreement with the experimental observations.
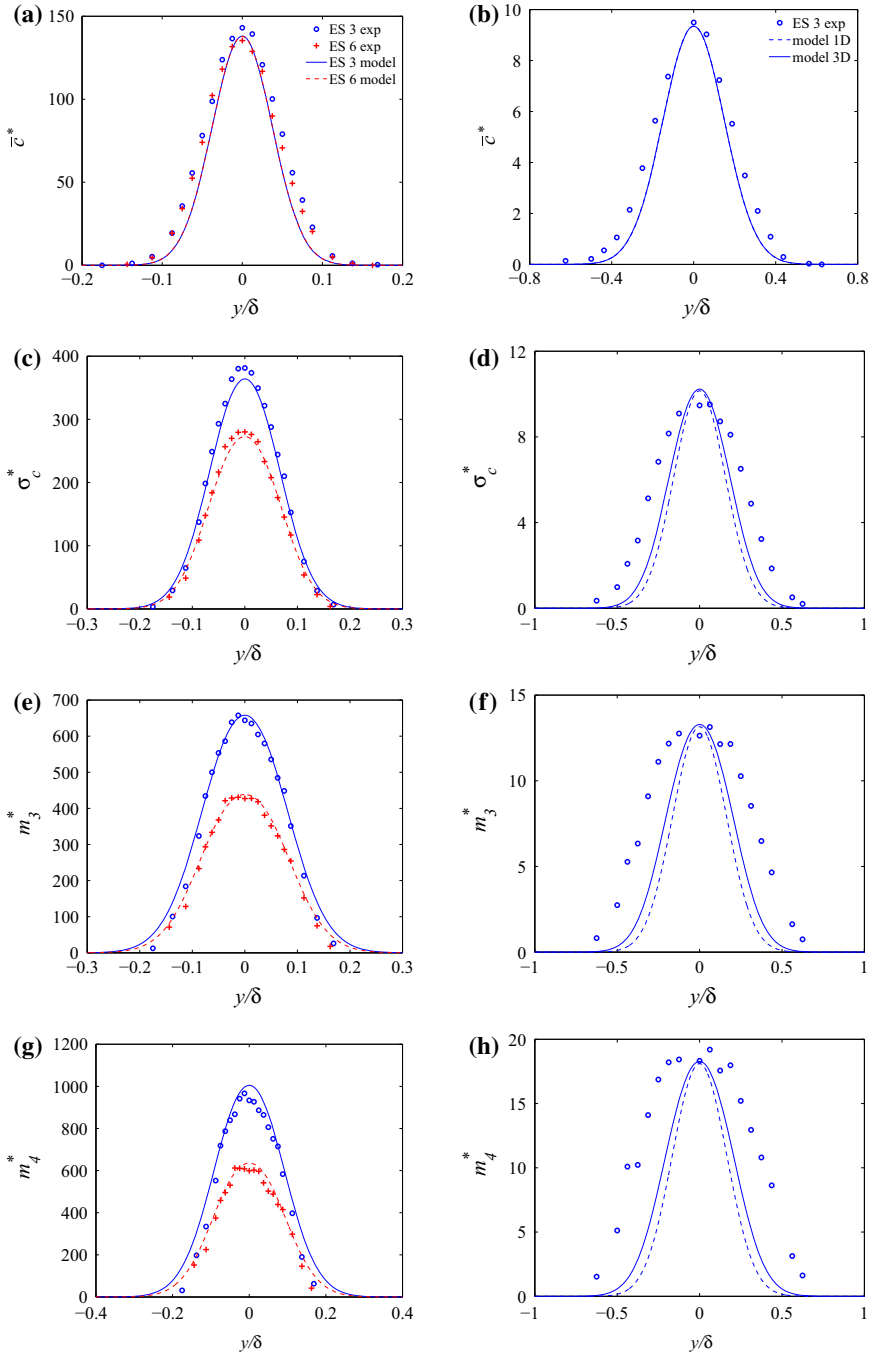
Fig. 7 ES case: comparison between experimental and modelled transverse profiles of the concentration statistics at source height and at $x/\delta = 0.625$: **a** $\bar{c}^*$, **c** σ_c^*, **e** m_3^*, **g** m_4^*, and at $x/\delta = 3.75$: **b** $\bar{c}^*$, **d** σ_c^*, **f** m_3^*, **h** m_4^*. *Blue circles* experimental values for ES 3, *red crosses* experimental values for ES 6, *blue solid line* and *red dash line* solutions provided by Eq. 27, *blue dash line* solutions provided by Eq. 21. Note that at $x/\delta = 0.625$ the differences between the solutions computed by means of Eq. 21 and Eq. 27 are negligible
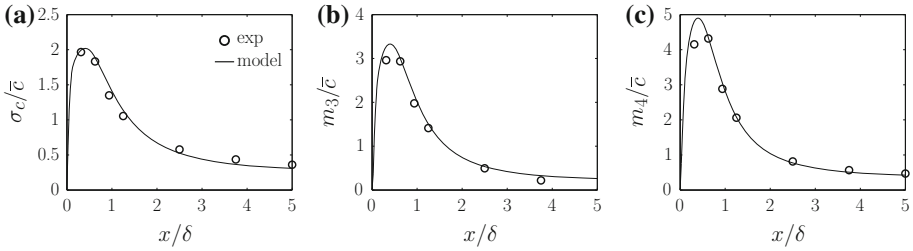
Fig. 8 LLS case: concentration statistics vs x/δ at $y/\delta = 0$, $z/\delta = z_s/\delta$: **a** $\sigma_c/\overline{c}$, **b** $m_3/\overline{c}$, **c** $m_4/\overline{c}$

As we proceed downwind from the source, the results show a slight deterioration, which is only partially corrected by adopting a 3-D model of i_{cr}. In Fig. 7b, d, f, and h we show a comparison between experimental and analytical results for the ES 3 emission, computed with both the 1-D and the 3-D models of i_{cr} (Eq. 25) at $z/\delta = z_s/\delta$ and $x/\delta = 3.75$, where the influence of the source size has become negligible. The model provides quite accurate estimates of the concentration statistics, even though the spreads of the simulated profiles of m_3^* and m_4^* are narrower than the experimental profile.

4.2 Low-Level Source

As for the ES case, the modelled profiles of the second-, third- and fourth-order moments of the concentration as function of the x-coordinate at $y = 0$ and $z = z_s$ (Fig. 8) present a fairly good agreement with the experimental data, both close to the source and in the far field.

Even in this case the predictions performed through 1-D and 3-D formulations of i_{cr} provide good results of the concentration statistics close to the source, given the ζ_y coefficient is next to zero up to $x/\delta \approx 0.5$ (see Fig. 4). This is shown in Fig. 9a, c, e, and g, where we have plotted the transverse profiles of the concentration statistics at the source height.

In the far field, the model with $i_{cr} = i_{cr}(x)$ is not able to reproduce the profiles of the concentration statistics, even qualitatively. As Fig. 9d, f, and h show, the model fails to reproduce the off-centreline peaks and the transverse profiles keep a Gaussian shape. In order to improve the model prediction it is then necessary to assume $i_{cr} = i_{cr}(x, y, z)$. The results of the model are however less accurate than in the ES case. In the far field, the model underestimates the mean concentration peak on the plume axis (Fig. 9b), due to the discrepancies between the modelled σ_y (Eq. 15) and its experimental values (Nironi et al. 2015). The transverse profiles of the higher order moments show the emergence of off-centreline peaks, that are particularly marked for the third order moment. The model captures these tendencies qualitatively but its quantitative predictions show significant discrepancies with the experimental data (Fig. 9d, f, h).

5 Error and Sensitivity Analysis

Finally, we evaluate the reliability and robustness of the fluctuating plume model by means of:

- estimates of its global accuracy, computed through a comparison between the measured and computed concentration statistics;
- a Monte-Carlo analysis providing the sensitivity of the solutions to variations of the key parameters.
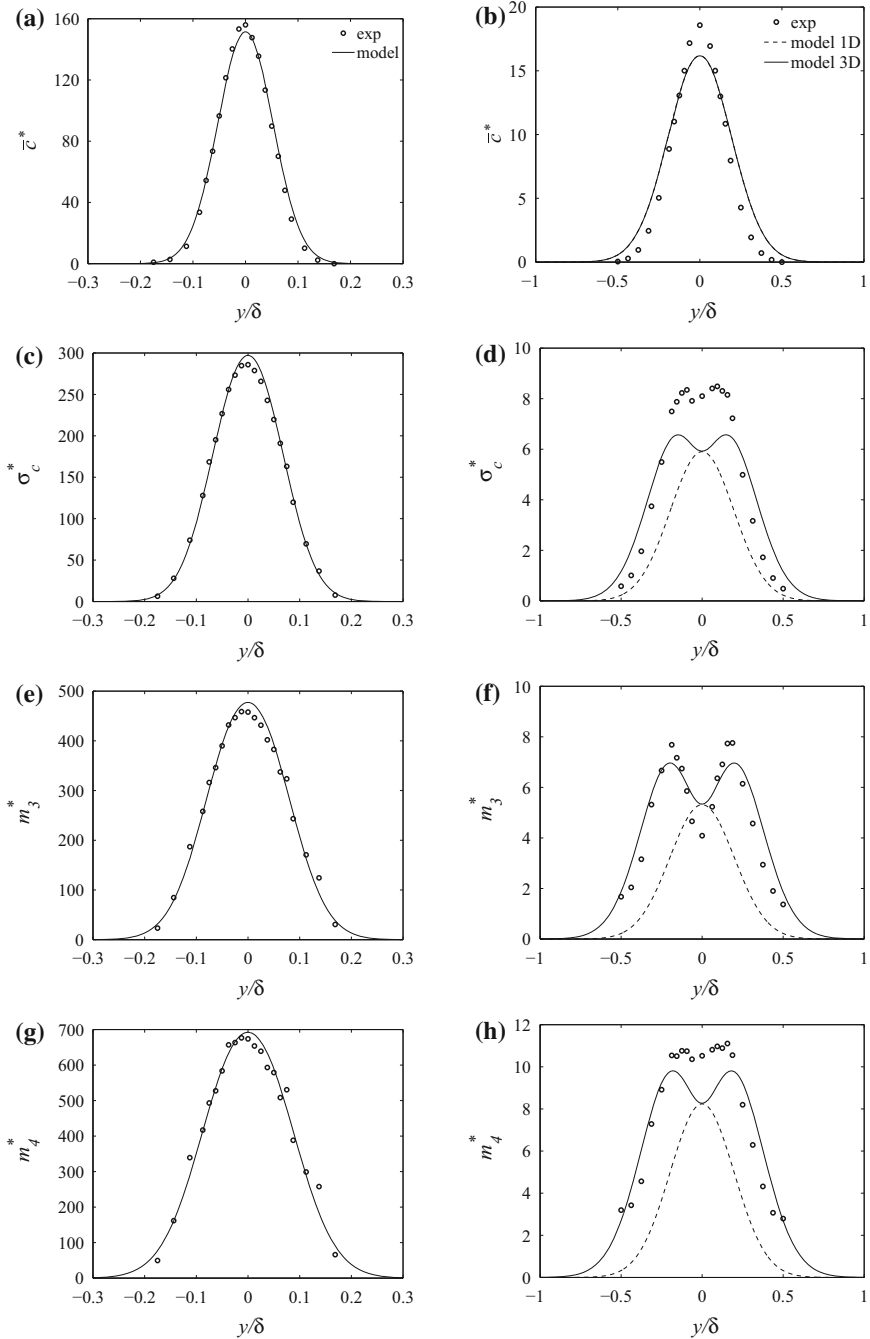
Fig. 9 LLS case: comparison between experimental and modelled transverse profiles of the concentration statistics at the source height and at $x/\delta = 0.625$: **a** $\overline{c}^*$, **c** σ_c^*, **e** m_3^*, **g** m_4^*, and at $x/\delta = 3.75$: **b** $\overline{c}^*$, **d** σ_c^*, **f** m_3^*, **h** m_4^*. *Circles* experimental values, *solid line* solutions provided by Eq. 27, *dash line* solutions provided by Eq. 21. Note that at $x/\delta = 0.625$ the differences between the solutions computed by means of Eq. 21 and Eq. 27 are negligible
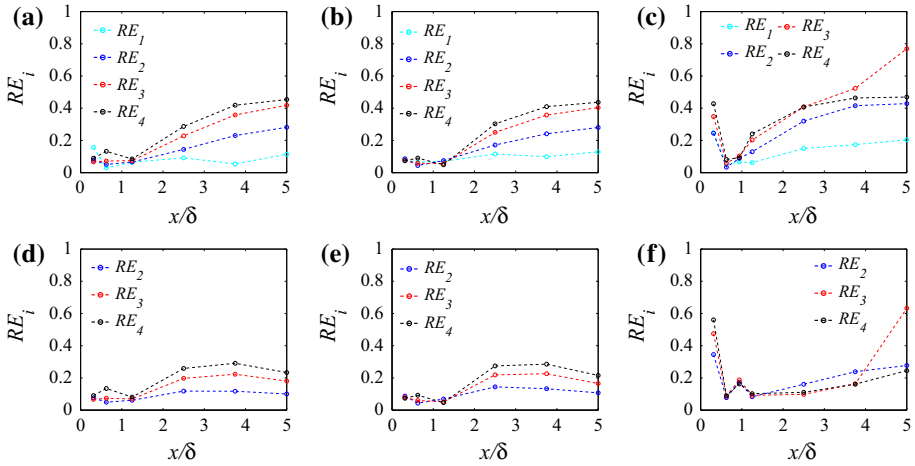
Fig. 10 Relative error of the transversal profiles vs x/δ for 1-D model of i_{cr}: **a** ES 3, **b** ES 6, **c** LLS; and 3-D model of i_{cr}: **d** ES 3, **e** ES 6, **f** LLS

5.1 Errors

To investigate the reliability of the model we need to quantify the gap between the measured, $(m_i^*)_{exp}$ and the computed $(m_i^*)_{mod}$ values of the moments of the concentration. To this end we define the relative error as

$$RE_i = \sqrt{\frac{\int \left[(m_i^*)_{mod} - (m_i^*)_{exp}\right]^2 \, ds}{\int \left[(m_i^*)_{exp}\right]^2 \, ds}}, \tag{34}$$

with $i = 1, 2, 3, 4$, $ds = dy, dz$ and where i is the moment number.

The analysis is performed considering the cases of i_{cr} parametrized by the 1-D model (Eq. 23c) and the 3-D model (Eq. 25). Figure 10a–c show that the relative error associated to the mean concentration RE_1 takes low values across the whole domain. Conversely RE_2, RE_3 and RE_4 computed for 1-D i_{cr} model are bounded close to the release point, but they increase significantly away from it.

The relative errors evaluated for 3-D i_{cr} model are reported in Fig. 10d–f, where RE_1 is not plotted, since it does not depend on the formulation of i_{cr}. RE_i of the transversal profiles are bounded in all the cases, except for RE_3 in the LLS case (Fig. 10f). This is due to the particular shape of the experimental profile of m_3^* at $x = 5\delta$, that exhibits significant off-centreline peaks. As shown in Fig. 9f, the model reproduces this behaviour only qualitatively, but it fails in quantifying the centreline values of m_3^*.

In the light of this analysis, we can however conclude that, by adopting a suitable parametrization of i_{cr}, the model reproduces the statistics of the concentration field produced by a fluctuating plume with good accuracy.

5.2 Sensitivity Analysis

In order to discuss the reliability of the model for operational purposes, we analyze its sensitivity to several key parameters, whose evaluation is potentially affected by non-negligible errors. Our analysis focuses on two main features. Firstly, we discuss the uncertainties related

Table 5 Turbulent velocity field at $\overline{z}_m$ and z_s

	$\overline{u}$ (m s^{-1})	σ_v (m s^{-1})	σ_w (m s^{-1})	ε (m^2 s^{-3})
$\overline{z}_m = 0.14\delta$	3.2	0.28	0.23	0.18
$z_s = 0.06\delta$	2.6	0.29	0.22	0.38

to the reference value of the vertical coordinate at which are evaluated the velocity statistics used to compute the model parameters. Secondly, we analyze the errors induced by uncertainties in the parametrizations of i_{cr}.

In the results presented in Sect. 4, velocity statistics, i.e. $\overline{u}_m$, σ_v, σ_w and ε, were evaluated at the plume centroid $z = \overline{z}_m$, which varies with the distance from the source. A simpler approach consists of estimating these same quantities at a fixed reference height, generally the source elevation z_s. As an example, we show in Table 5 the differences of these velocity statistics in the far field ($x/\delta = 3.75$) for the LLS emission, as computed at z_s and $\overline{z}_m$ (in this case $\approx 2.5 z_s$). As shown in Table 5 the two parameters that exhibit higher variations are $\overline{u}_m$ and ε. Comparisons of the concentration statistics computed at $x/\delta = 3.75$ for the LLS case, and adopting these two different sets of input data, are plotted in Fig. 11a–c. Results clearly show that these variations in the input data affect significantly the model performances and produce differences in the standard deviation and the third- and fourth-order moments of the concentration exceeding 100 %.

As a second step, we investigate the sensitivity on the parametrization of i_{cr} (Eq. 23c). Since the spatial distribution of the concentration fluctuations downwind the source is highly influenced by the emission conditions (Nironi et al. 2015), i.e. source size and elevation, the determination of a suitable longitudinal profile of i_{cr} represents actually the main modelling challenge. To test the influence of uncertainties in the parametrization of i_{cr} we performed a Monte-Carlo simulation, assuming that the coefficients in Eq. 23c are normally distributed, with averages values given by the reference values reported in Table 2 and a standard deviation corresponding to 10 % of the average. These turn out to be a maximum close to the source (≈ 15 %) and a minimum far from it (≈ 10 %). The variations of the second-, third- and fourth-order moments are shown in Fig. 11d–f and attain a maximal value ≈ 20 %.

The same analysis was performed for the parameters ζ_y and ζ_z (see Eq. 25) characterizing the evolution of i_{cr} in the transversal and vertical directions. These were assumed to be normally distributed, with a standard deviation equal to 10 % of the mean values reported in Table 3. The resulting uncertainties in the vertical profiles of the high order concentration statistics at $x/\delta = 0.625$ for the LLS case are plotted in Fig. 11g–i. These show that variations of these parameters have little influence on σ_c^* (Fig. 11g) and m_3^* (Fig. 11h) whereas they can induce significant variations in the m_4^* profiles (Fig. 11i), especially at the plume edges.

6 Discussion and Conclusion

We have investigated the reliability of a meandering plume model to simulate the dispersion of a passive scalar emitted within a neutral turbulent boundary layer. Following most authors who presented a similar model (Sawford and Stapountzis 1986; Yee et al. 1994; Luhar et al. 2000; Cassiani and Giostra 2002; Franzese 2003), we base its formulation on two main assumptions. The first is that the dispersion of the plume centre of mass and that of the tracer particles around it are statistically independent. The second is that both dispersion processes
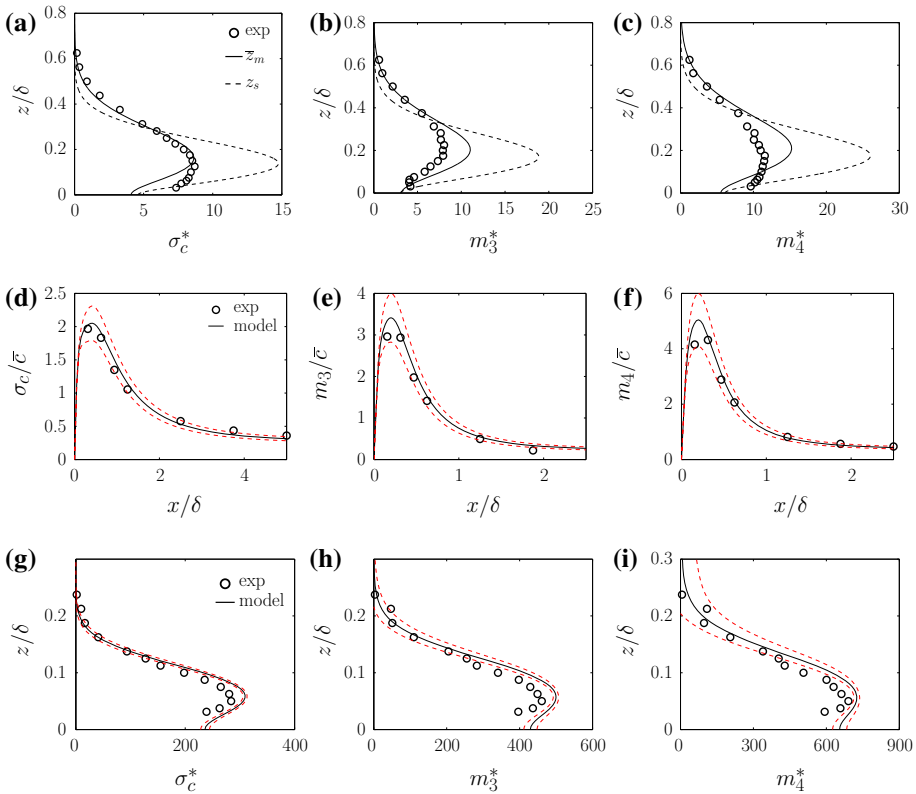
Fig. 11 Sensitivity analysis for the LLS case. Influence of the plume centroid on the vertical profiles of the concentration statistics, $x/\delta = 3.75$, $y = 0$: **a** σ_c^*, **b** m_3^*, **c** m_4^*; *circles* experiments; *solid line* model with $\overline{u}(\overline{z}_m)$, $\sigma_v(\overline{z}_m)$, $\sigma_w(\overline{z}_m)$, $\varepsilon(\overline{z}_m)$; *black dash line* model with $\overline{u}(z_s)$, $\sigma_v(z_s)$, $\sigma_w(z_s)$, $\varepsilon(z_s)$. Influence of an uncertainty of ± 10 % in the estimate of the coefficients of i_{cr} (Table 2) on the longitudinal profiles of the concentration statistics at $y/\delta = 0$, $z/\delta = z_s/\delta$: **d** $\sigma_c/\overline{c}$, **e** $m_3/\overline{c}$, **f** $m_4/\overline{c}$. Influence of an uncertainty of ± 10 % in the estimate of the coefficient ζ_z (Table 3) on the vertical profiles of the concentration statistics at $y/\delta = 0$, $x/\delta = 0.625$: **g** σ_c^*, **h** m_3^*, **i** m_4^*. The uncertainty is evaluated as the ratio between the standard deviation and the mean value and it is represented by *red dash lines*

are given by motions in the vertical and transversal plane that are decoupled one from the other. The first assumption is actually verified only close to the source and in the far field. The second cannot be strictly justified on some physical basis. It is rather adopted since it allows simplification of the model formulation.

A fluctuating plume model requires the setting of several parameters. According to our formulations, these are C_0 and C_r, the Kolmogorov and Richardson–Obukhov constants, respectively, α_T, required to evaluate the time scales T_{my} and T_{mz} characterizing the intensity of the meandering downwind the source, and the parameters needed to model the spatial evolution of the intensity of the relative concentration fluctuations i_{cr} in the longitudinal direction and in the transversal planes (α_1, α_2 and α_3). All these parameters were set by systematically comparing our model results to the experimental data presented in Nironi et al. (2015), in particular concerning the Eulerian integral length scales, the total plume spreads σ_y and σ_z and the spatial distribution of i_c. Furthermore, the information provided by this experimental dataset was used here to verify the consistency of the model formulation, as

well as of the procedure adopted to tune its parameters, with the main features characterizing the physics of the dispersion process.

We have then tested the performances of the model by comparing its solutions with experimental profiles of the higher-order moments of the concentration PDF (Nironi et al. 2015). The comparison shows that, despite the theoretical weakness of some of its basic assumptions, once properly set the governing parameters, the meandering model is able to predict the concentration statistics with a suitable accuracy and to simulate the effects due to the source size and elevation. In the near field, a good accuracy of the results could be achieved assuming a constant i_{cr} on the yz-planes. The good agreement between model simulations and experimental data persists even at larger distances from the source, where the assumption of the statistical independence of the meandering and the relative dispersion, as well as of the vertical and transversal motions, is far from being verified. Finally, in the far field, as the relative dispersion becomes the only relevant dispersion mechanism, the 1-D model results progressively deteriorate. To reliably reproduce profiles of the higher-order moments, the model requires a more complex formulation of i_{cr}, which takes account for its variability along the transverse and vertical directions.

In view of the application of the model for operational purposes, we have finally tested its sensitivity to the variations of several key parameters. The analysis shows that the model performances can be significantly affected by varying the reference values of the height from the ground at which the velocity statistics are estimated. Furthermore, the model is shown to exhibit also a strong sensitivity on the parametrization of i_{cr}, especially in the near field.

This sensitivity of the model to parametrization of i_{cr} represents, in our opinion, the main limitation for its use for operational purposes, since the spatial distribution of i_{cr} is strictly linked to that of i_c. As widely discussed in Nironi et al. (2015), the evolution of i_c is highly influenced by the conditions at the emissions. These include the source elevation and diameter and the emission velocity, as well as other features characterizing the source design that can affect the flow dynamics in the wake of the source, where most of the production of the concentration variance takes place. All these aspects influencing the plume dynamics in its initial phase of growth can not realistically be fully characterized when applying the model to atmospheric emissions. As a consequence, estimates of the higher-order concentration statistics in this near-field region can be affected by significant uncertainties.

Given these uncertainties of the model results in real case studies and in the light of the findings presented in Nironi et al. (2015), a last remark can be made. As long as the Gamma distribution was shown to reliably model the concentration PDF (independently of the emission conditions), it is actually questionable if, for operational purposes, the concentration statistics deserve to be computed by a meandering plume model, that requires several input parameters, rather than with more simple semi-empirical models. These should be formulated in order to provide solely estimates of $\bar{c}$ and i_c, the two independent quantities needed to fix the form of the Gamma distribution, which can be subsequently used to compute the higher-order moments.

References

Amicarelli A, Salizzoni P, Leuzzi G, Monti P, Soulhac L, Cierco FX, Leboeuf F (2012) Sensitivity analysis of a concentration fluctuation model to dissipation rate estimates. Int J Environ Pollut 48:164–173

Arya PS (1999) Air pollution meteorology and dispersion. Oxford University Press, Oxford, 310 pp

Biferale L, Boffetta G, Celani A, Devenish BJ, Lanotte A, Toschi F (2005) Lagrangian statistics of particle pairs in homogeneous isotropic turbulence. Phys Fluids 17:115101/1–115101/9

Boffetta G, Sokolov I (2002) Relative dispersion in fully developed turbulence: the Richardson's law and intermittency corrections. Phys Lett 88:094501/1–094501/4

Cassiani M (2013) The volumetric particle approach for concentration fluctuations and chemical reactions in Lagrangian particle and particle-grid models. Boundary-Layer Meterol 146:207–233

Cassiani M, Franzese P, Giostra U (2005) A PDF micromixing model of dispersion for atmospheric flow. Part I: Development of the model, application to homogeneous turbulence and neutral boundary layer. Atmos Environ 39:1457–1469

Cassiani M, Giostra U (2002) A simple and fast model to compute concentration moments in a convective boundary layer. Atmos Environ 36:4717–4724

Fackrell JE, Robins AG (1982) The effects of source size on concentration fluctuations in plumes. Boundary-Layer Meteorol 22:335–350

Ferrero E, Mortarini L, Alessandrini S, Lacagnina C (2013) Application of a bivariate gamma distribution for a chemically reacting plume in the atmosphere. Boundary-Layer Meteorol 147:123–137

Franzese P (2003) Lagrangian stochastic modeling of a fluctuating plume in the convective boundary layer. Atmos Environ 37:1691–1701

Franzese P, Cassiani M (2007) A statistical theory of turbulent relative dispersion. J Fluid Mech 571:391–417

Gailis RM, Hill A, Yee E, Hilderman T (2007) Extension of a fluctuating plume model of tracer dispersion to a sheared boundary layer and to a large array of obstacles. Boundary-Layer Meterol 607:577–607

Gifford F (1959) Statistical properties of a fluctuating plume dispersion model. Adv Geophys 6:117–137

Ishihara T, Kaneda Y (2002) Relative diffusion of a pair of fluid particles in the inertial subrange of turbulence. Phys Fluids 14:L69–L72

Leuzzi G, Amicarelli A, Monti P, Thomson DJ (2012) A 3D Lagrangian micromixing dispersion model LAGFLUM and its validation with a wind tunnel experiment. Atmos Environ 54:117–126

Luhar AK, Hibberd MF, Borgas MS (2000) A skewed meandering plume model for concentration statistics in the convective boundary layer. Atmos Environ 34:3599–3616

Monin AS, Yaglom AM (1971) Statistical fluid mechanics, vol 1. MIT Press, Cambridge, 769 pp

Mortarini L, Franzese P, Ferrero E (2009) A fluctuating plume model for concentration fluctuations in a plant canopy. Atmos Environ 43:921–927

Nironi C, Salizzoni P, Marro M, Mejan P, Grosjean N, Soulhac L (2015) Dispersion of a passive scalar fluctuating plume in a turbulent boundary layer. Part I: Velocity and concentration measurements. Boundary-Layer Meteorol

Obukhov AM (1941) On the distribution of energy in the spectrum of turbulent flow. Izv Akad Nauk USSR, Ser Geogr Geofiz 5:453–466

Ott S, Mann J (2000) An experimental investigation of the relative diffusion of particle pairs in three-dimensional turbulent flow. J Fluid Mech 422:207–223

Reynolds AM (2000) Representation of internal plume structure in Gifford's meandering plume model. Atmos Environ 34:2539–2545

Richardson LF (1926) Atmospheric diffusion shown on a distance-neighbour graph. Proc R Soc Lond 110:709–737

Sawford B (2004) Micro-mixing modelling of scalar fluctuations for plumes in homogeneous turbulence. Flow Turbul Combust 72:133–160

Sawford B, Stapountzis H (1986) Concentration fluctuations according to fluctuating plume models in one and two dimensions. Boundary-Layer Meteorol 37:89–105

Tennekes H (1982) Similarity relations, scaling laws and spectral dynamics. In: Niewstadt F, Van Dop H (eds) Atmospheric turbulence and air pollution modelling. D. Reidel Publishing Company, Dordrecht, pp 37–68

Vinkovic I, Aguirre C, Simoëns S (2006) Large-eddy simulation and Lagrangian stochastic modeling of passive scalar dispersion in a turbulent boundary layer. J Turbul 7:1–14

Xie Z, Hayden P, Voke PR, Robins AG (2004) Large-eddy simulations of dispersion: comparison between elevated and ground level sources. J Turbul 5:1–16

Yee E, Chan R, Kosteniuk PR, Chandler GM, Biltoft CA, Bowers JF (1994) Incorporation of internal fluctuations in a meandering plume model of concentration fluctuations. Boundary-Layer Meteorol 67:11–39

Yee E, Wilson DJ (2000) A comparison of the detailed structure in dispersing tracer plumes measured in grid-generated turbulence with a meandering plume model incorporating internal fluctuations. Boundary-Layer Meteorol 94:253–296